Molecular Electric Quadrupole Moment, Magnetic Susceptibility Tensor and Deuterium Quadrupole Coupling Constant in Cyanoacetylene

W. H. Stolze and D. H. Sutter

Abteilung Chemische Physik im Institut für Physikalische Chemie der Universität Kiel

Z. Naturforsch. **39a**, 1092–1103 (1984); received August 30, 1984

The rotational Zeeman effect in the $J \rightarrow J' = 0 \rightarrow 1$ and $1 \rightarrow 2$ rotational transitions has been observed for H–C≡C–C≡^{14}N, D–C≡C–C≡^{14}N, D–C≡C–C≡^{15}N, and H–C≡C–C≡^{15}N using a microwave bridge superheterodyne spectrometer. From the experimental $g_\perp$-values, susceptibility anisotropies and rotational constants, the molecular electric quadrupole moment, which plays an important role for collisional excitation and relaxation, follows as $Q_\parallel = 2.14(9) \times 10^{-26}$ esu cm^2 (referred to the center of mass of the H–C≡C–C≡^{14}N species).

Since the Deuterium quadrupole hyperfine splittings in the Zeeman spectra could be resolved, it was also possible to fit the Deuterium quadrupole coupling constant. Our value, $eqQ(^2\mathrm{H}) = 198.2(46)$ kHz is about 10% smaller than the value derived from a recent high resolution microwave Fourier transform study. The reasons for this discrepancy are discussed.

All experimental molecular parameters are compared to the results of ab initio quantum chemical calculations and it is argued that the ^{14}N nuclear electric quadrupole moment is possibly about 30% larger than presently assumed.

Introduction

The first microwave spectroscopic study of HCCCN dates back to the years 1949 to 1950, when Westenberg and Bright Wilson jr. [1] investigated the $J = 2 \rightarrow J = 3$ rotational transitions of ten different isotropic species in the K-band region. They also obtained a first value for the ^{14}N-quadrupole coupling constant from the HFS splittings of the most abundant species and they got a first value for the molecular electric dipole moment from the Stark effect splittings in an exterior electric field.

When in 1971 Turner reported the observation of the $J = 1$ to $J = 0$ rotational emission line in the Sagittarius B2 galactic radio source [2], radio astronomers and astrophysicists immediately became interested in this molecule, and only five years later seventeen galactic sources were known [3] with the $J = 1$ to $J = 0$ transition in SgrB2, probably a weak maser. In 1978 Churchwell, Winnewisser and Walmsley [4] observed a strong emission signal of the $1 \rightarrow 0$ transition from a small region of the Taurus molecular cloud 1, which, as they think, might be an example for star formation on a small scale.

Quite recently Dreizler and coworkers [5, 5a] have observed and analysed the Deuterium coupling in D–C≡C–C≡^{15}N and in D–C≡C–C≡^{14}N by means of the high sensitivity high resolution technique of microwave Fourier transform spectroscopy, and ab initio calculations of molecular properties of Cyanoacetylene and the higher Cyanopolyenes, carried out on the (3-21 G)- and (6-31 G**)-levels, have been published by Ha and Nguyen [6]. The latter are ideally suited for comparison with precise microwave spectroscopic data.

In the following we report the results of a high resolution rotational Zeeman effect study [7, 8, 9] of Cyanoacetylene [10]. Such a study leads to the molecular $g_\perp$ value and the anisotropy of the molecular magnetic susceptibility tensor $\chi_\perp - \chi_\parallel$. From those – via their theoretical expressions [11] – it is possible to derive the second moments of the electron charge distribution and the molecular electric quadrupole moment, quantities which can be used to probe the accuracy of quantum chemical ab initio wave functions in the outer regions of a molecule.

The knowledge of the molecular electric quadrupole moment is also of direct interest for the

Reprint requests to Prof. Dr. D. H. Sutter, Institut für Physikalische Chemie der Universität Kiel, Olshausenstr. 40, D-2300 Kiel.

0340-4811 / 84 / 1100-1092 $ 01.30/0. – Please order a reprint rather than making your own copy.

analysis and interpretation of collisional excitation and relaxation of rotational energy since it opens – quite effectively [12] – $\Delta J = \pm 2$ relaxation channels.

Finally the strong magnetic field (about 2 Tesla) uncouples Deuterium spin and overall rotation. This leads to doublet splittings of the Zeeman satellites with intensity ratios 2 ($M_I = \pm 1$ states) to 1 ($M_I = 0$ states). Since these splittings are essentially determined by the Deuterium quadrupole coupling constant, it is possible to derive an independent value for the latter.

Measurements and Analysis of the Data

Cyanoacetylene and its isotopic species were prepared as described in [5] using Propynoic Acid Methylester as starting material. The samples were stored at liq. N_2 temperatures. While the ^{1}H-species appeared to be stable in our brass waveguide absorption cells, the absorption lines of the ^{2}H-species dwindled at the beginning and became stable only after several fillings. Appearently a proton exchange occurs with water molecules adsorbed at the wall. The decay indicates a lifetime on the order of minutes. In other words, every 10^6-th to 10^7-th wall collision leads to a proton (deuteron) exchange, and the appearent stability of the molecule is better described as the steady state of the corresponding exchange reaction scheme.

The microwave bridge superheterodyne spectrograph [13, 14] and high field electromagnet [15, 16] used in this study have been described previously. Using the appropriate mixers and waveguide components, the frequency range of the system was extended down to 7.5 GHz. The bridge itself consists of two identical J-band brass cells of 1.80 m effective length. The use of a POLARAD 1208e Klystron signal source as local oscillator slightly improved the signal to noise ratios. Typical recording conditions were: pressures below 1 mTorr (0.12 Pa), cell temperatures about $-50\,^\circ$C, microwave power in the sample arm below 0.1 μW.

Unter these conditions linewidths of 40 to 55 kHz (full width at half height) were obtained. In Fig. 1 we give an example. The observed linewidths are essentially caused by Doppler-broadening, wall collision broadening, and Stark-effect modulation broadening (7 kHz square wave modulation).

All Zeeman measurements were carried out at fields close to $18.9 \cdot 10^3$ Gauß. To account for the longitudinal inhomogeneity of the magnetic field, the field profile was measured in every experiment and the average field value was used to analyse and simulate the spectra. This procedure is feasable since the spectra are essentially determined by the first order Zeeman effect [17]. The calibration uncertainty of the Rawson Lush rotating coil Gaußmeter is on the order of 5 Gauß at 20 kG.

For the analysis of the spectra we have used the effective Hamiltonian

$$\hat{\mathscr{H}}_{\text{eff}} = \hat{\mathscr{H}}_{\text{rot}} + \sum_{i}^{\substack{\text{quadrupole}\\ \text{nuclei}}} \hat{\mathscr{H}}_{\text{Q},i} + \sum_{i}^{\substack{\text{quadrupole}\\ \text{nuclei}}} \hat{\mathscr{H}}_{\text{g},i} + \hat{\mathscr{H}}_{\text{g}} + \hat{\mathscr{H}}_{\chi} + \sum_{i}^{\substack{\text{quadrupole}\\ \text{nuclei}}} \hat{\mathscr{H}}_{\text{SR},i}. \tag{1}$$

In (1) $\hat{\mathscr{H}}_{\text{rot}}$ is the standard rigid rotor Hamiltonian, $\hat{\mathscr{H}}_{\text{Q},i}$ ($i = 1, 2$), if applicable, are the nuclear quadrupole interaction Hamiltonians for up to two quadrupole nuclei (^{14}N and ^{2}H), $\hat{\mathscr{H}}_{\text{g},i}$ are the nuclear Zeeman effect Hamiltonians for the quadrupole nuclei, $\hat{\mathscr{H}}_{\text{g}}$ and $\hat{\mathscr{H}}_{\chi}$ are the first and second order molecular Zeeman effect Hamiltonians, and $\hat{\mathscr{H}}_{\text{SR},i}$ are the spin-rotation Hamiltonians, which account for the interaction of the nuclear magnetic moments of the ^{2}H or ^{14}N nucleus with the intramolecular magnetic field produced by the overal rotation of the molecular charge distribution. The Hamiltonian matrix corresponding to (1) was set up in the uncoupled basis $|J, M_J, I_{(^{14}\text{N})}, M_{(^{14}\text{N})}, I_{(^2\text{H})}, M_{(^2\text{H})}\rangle$ etc. and was diagonalized numerically.

For the matrix elements the reader is referred to Appendix I of [18], where the corresponding symmetric top matrix elements are listed. From those the linear rotor matrix elements are obtainable simply by setting $K = 0$. All matrix elements which are off-diagonal in J, were neglected. By a second order perturbation treatment their contribution may be estimated to be below 1 kHz, which is still small as compared to the resolution power of the spectrograph. To calculate relative intensities of the Zeeman satellites, the molecular electric dipole moment direction cosine matrix elements were subjected to the unitary transformation corresponding to the diagonalization procedure described above. Double precision calculation on a DEC PDP 10

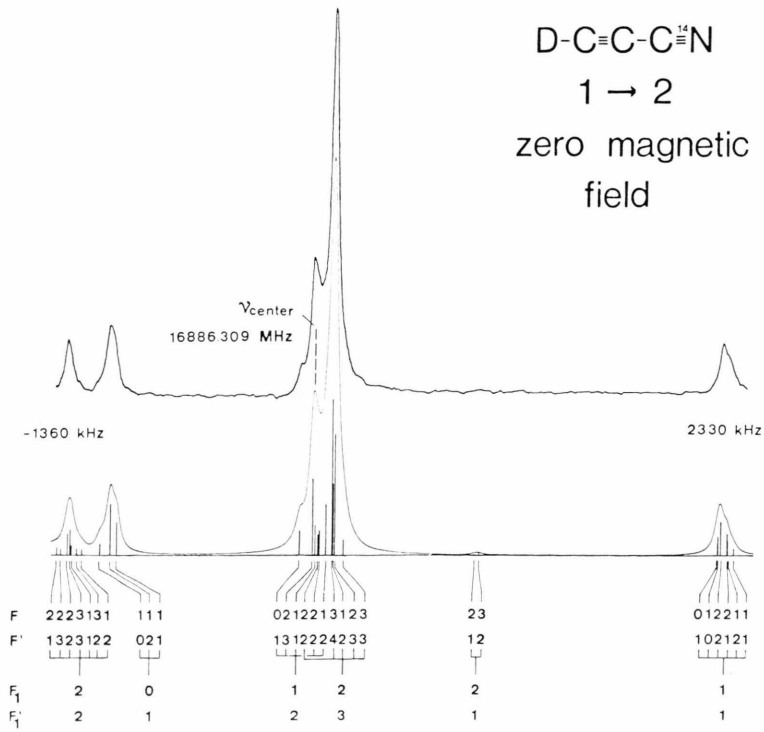

Fig. 1a. Zero field nuclear quadrupole hyperfine pattern of the $J = 1 \rightarrow J = 2$ rotational transition in D−C≡C−C≡^{14}N. To designate the states we use the following coupling scheme (compare text): First ^{14}N-spin and rotational angular momentum are coupled to form the intermediate angular momenta F_1 (lower level) and F_1' (upper level). Second the intermediate angular momentum and Deuterium spin are coupled to the final angular momentum F (lower level) and F' (upper level). The intensities follow from the corresponding transformation of the electric dipole transition matrix element.

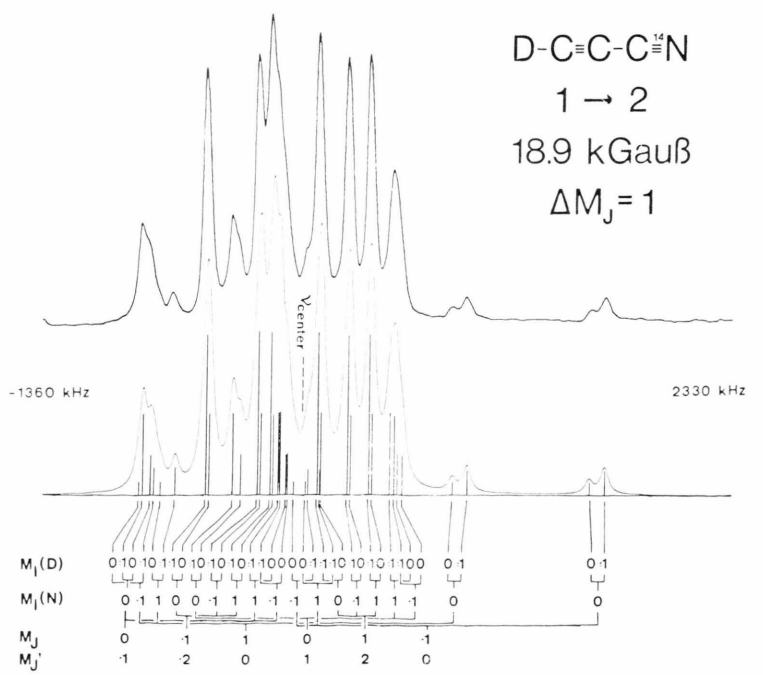

Fig. 1b. Zeeman-HFS-pattern of the $J = 1 \rightarrow J = 2$ rotational transition of D−C≡C−C≡^{14}N observed at a field of 18.9 kGauß (1.89 Tesla). Since the magnetic field effectively uncouples spins and rotational angular momentum, the quantum numbers of the uncoupled representation $|J, M_J, I_{(^{14}N)}, M_{(^{14}N)}, I_{(D)}, M_{(D)}\rangle$ are used to designate the upper and lower states. The computer simulation (lower trace) was calculated from the molecular constants given in Table 5, the nuclear g_I-values [27], and the spin-rotation coupling constants [23] as described in the text. The two low intensity doublets at far right with intensity ratio 1 ($M_{(D)} = 0$; left satellite) to 2 ($M_{(D)} = \pm 1$; right satellite) are caused by the Deuterium nuclear quadrupole coupling.

Computer (i.e. 19 significant figures) was used throughout.

For the calculation of the zero field spectra we also used a separate program in which the Hamiltonian matrix is set up in a coupled basis. In a first step the overall angular momentum J is coupled to the ^{14}N-spin $I_{(^{14}N)}$ (if applicable) to form the intermediate angular momentum F_1 and in a second step the ^{2}H-spin (if applicable) is coupled to the intermediate angular momentum to form the final overall angular momentum F. In Fig. 1a the zero field lines of the D−C≡C−C≡^{14}N species are labelled with the quantum numbers F_1, F which correspond to this coupling scheme. In Tables 1 through 4 we give the observed frequencies. They were used to fit the molecular parameters listed in Table 5.

Derived Molecular Parameters

In the following we use the theoretical rigid rotor expressions for the $g_\perp$-values and the susceptibilities $\chi_\perp$ and $\chi_\parallel$ to derive "experimental" values for the molecular electric quadrupole moment, the so called diamagnetic and paramagnetic susceptibilities and the second moments of the electron charge distributions. As discussed in some detail in Chapt. II B of [9], the results should come close to the corresponding vibrational ground state expectation values. For conveniance of the reader, the relevant expressions [11a, 11b] are given below in (2) to (10).

Theoretical rigid rotor expressions for $g_\perp$, $\chi_\perp$ and $\chi_\parallel$

$$g_\perp = \frac{m_p}{I_\perp}\left(\sum_{\nu}^{\text{nuclei}} Z_\nu z_\nu^2 + \frac{2}{m}\left(\frac{L_x L_x}{\Delta}\right)\right) = \frac{m_p}{I_\perp}\left(\sum_{\nu}^{\text{nuclei}} Z_\nu z_\nu^2 + \frac{2}{m}\left(\frac{L_y L_y}{\Delta}\right)\right), \tag{2}$$

$$\chi_\perp = -\frac{e^2}{4m c^2}\left(\langle 0|\sum_{\varepsilon}^{\text{electrons}}(x_\varepsilon^2 + z_\varepsilon^2)|0\rangle + \frac{2}{m}\left(\frac{L_y L_y}{\Delta}\right)\right) = -\frac{e^2}{4m c^2}\left(\langle 0|\sum_{\varepsilon}^{\text{electrons}}(y_\varepsilon^2 + z_\varepsilon^2)|0\rangle + \frac{2}{m}\left(\frac{L_x L_x}{\Delta}\right)\right), \tag{3}$$

$$\chi_\parallel = -\frac{e^2}{4m c^2}\langle 0|\sum_{\varepsilon}^{\text{electrons}}(x_\varepsilon^2 + y_\varepsilon^2)|0\rangle. \tag{4}$$

The symbols have the following meaning m_p proton mass, m electron mass, Z_ν atomic number of the ν-th nucleus, $I_\perp$ molecular moment of inertia about any axis perpendicular to the linear heavy atom chain and running through the center of mass, z_ν z-coordinate of the ν-th nucleus (z-symmetry axis of the molecule), x_ε, y_ε, z_ε coordinates of the ε-th electron, e elementary charge (proton charge), c velocity of

Table 1. Zeeman splittings observed for HCCC^{15}N. ν_0 is the observed zero field frequency of the transition. ν_H is the frequency of the corresponding Zeeman-satellites designated by the M_J quantum numbers of the lower and upper state. The Zeeman splittings are calculated from the $g_\perp$-value and susceptibility anisotropy given in Table 8 as described in the text. Spinrotation coupling was neglected. Relativ intensities are in arbitrary units.

$J \to J'$ ν_0 (MHz) ΔM_J, H[Gauß]	$(\nu_H - \nu_0)$ exp. (kHz)	M_J	M'_J	rel. int.	$(\nu_H - \nu_0)$ calc. (kHz)	$\nu_{exp} - \nu_{calc}$ (kHz)
0 → 1 8833.507 MHz $\Delta M_J = 0$, 18808 G	141.0	0	0	100	139.7	1.3
0 → 1 8833.507 MHz $\Delta M_J = \pm 1$, 18815 G	−357.0 224.0	0 0	−1 1	50 50	−360.6 220.8	3.6 3.2
1 → 2 17666.998 MHz $\Delta M_J = 0$, 18889 G	−40.7 119.5	0 +/−1	0 +/−1	27 40	−40.2 120.7	−0.5 −1.2
1 → 2 17666.998 MHz $\Delta M_J = \pm 1$, 18888 G	−382.5 −319.5 −119.7 202.5 261.9 465.2	0 −1 1 0 1 −1	−1 −2 0 1 2 0	20 33 10 20 33 10	−382.4 −322.0 −120.8 201.3 261.6 462.9	−0.1 2.5 1.1 1.2 0.3 2.3

Table 2. Zeeman spectra of DCCC^{15}N. The magnetic field effectively uncouples Deuterium spin and overall rotation i.e. the uncoupled basis $|J, M_J, I, M_I\rangle$ gives excellent zeroth order wave functions. Thus J, M_J, and M_I are used to designate the states. Since the frequency of the incident radiation field is far above the NMR-resonance frequency, the molecules stay in their M_I states, i.e. $\Delta M_I = 0$ selection rule applies. However uncoupling of Deuterium spin and overall rotation is only approximate. This becomes appearent in the doublet splittings of $M_I = \pm 1$ satellites. Since the splitting is so close that the satellites cannot be resolved, their calculated average frequencies are used to fit the spectrum. The Zeeman splittings are calculated as described in the text from the $g_\perp$-value and susceptibility anisotropy listed in Table 5, the Deuterium quadrupole coupling constant given in Table 8, and the Deuterium g_I-value $g_I = 0.8574$ [27]. Nuclear shielding was neglected. In the last column we give the differences between the observed line peak frequencies and the calculated "average frequencies".

$J \rightarrow J'$ ν_0 (MHz) ΔM_J, H[Gauß]	$(\nu_H - \nu_{center})$ exp. [kHz]	M_J	M_J'	M_I(D)	rel. int.	$(\nu_H - \nu_{center})$ calc. [kHz]	$(\nu_H - \nu_{center})$ calc. average [kHz]	$\nu_{exp} - \nu_{calc.\,av.}$ [kHz]
$0 \rightarrow 1$	100.1	0	0	0	33	102.7	102.7	−2.6
8200.767 MHz	159.8	0	0	1	33	161.8	161.9	−2.1
$\Delta M_J = 0$, 18818 G		0	0	−1	33	161.9		
$0 \rightarrow 1$	−349.0	0	−1	1	50	−360.3	−350.3	1.3
8200.767 MHz		0	−1	−1	50	−360.1		
$\Delta M_J = \pm 1$, 18813 G		0	−1	0	50	−330.6		
	208.1	0	1	1	50	198.3	208.3	−0.2
		0	1	−1	50	198.5		
		0	1	0	50	228.0		
$1 \rightarrow 2$	−39.8	0	0	−1	27	−46.6	−40.9	1.1
16401.516 MHz		0	0	1	27	−46.6		
$\Delta M_J = 0$, 18889 G		0	0	0	27	−29.6		
	87.7	−1	−1	0	20	88.8	88.9	−1.2
		1	1	0	20	89.1		
	137.7	1	1	−1	20	139.6	139.7	−2.0
		1	1	1	20	139.6		
		−1	−1	−1	20	139.7		
		−1	−1	1	20	139.8		
$1 \rightarrow 2$	−376.2	0	−1	−1	20	−385.1	−372.4	−3.8
16401.516 MHz		0	−1	1	20	−385.1		
$\Delta M_J = \pm 1$, 18889 G		0	−1	0	20	−347.0		
	−307.3	−1	−2	−1	33	−315.2	−311.0	3.7
		−1	−2	1	33	−302.6		
	−155.2	1	0	0	10	−154.4	−154.4	−0.8
	−83.8	1	0	−1	10	−82.6	−82.6	−1.2
		1	0	1	10	−82.5		
	184.4	0	1	−1	20	175.6	188.2	−3.8
		0	1	1	20	175.6		
		0	1	0	20	213.6		
	247.7	1	2	−1	33	245.3	249.6	−1.9
		1	2	1	33	245.4		
		1	2	0	33	258.1		
	409.2	−1	0	0	10	406.4	406.4	2.8
	480.6	−1	0	−1	10	478.3	478.3	2.3
		−1	0	1	10	478.3		

light, L_x, L_y, L_x electronic angular momentum operators, i.e.

$$L_x = \frac{\hbar}{i} \sum_{\varepsilon}^{\text{electrons}} \left(y_\varepsilon \frac{\partial}{\partial z_\varepsilon} - z_\varepsilon \frac{\partial}{\partial y_\varepsilon} \right)$$

(and cyclic permutations),

$$\left\langle \frac{L_x L_x}{\Delta} \right\rangle = \sum_{n}^{\text{excited states}} \frac{\langle 0 | L_x | n \rangle \langle n | L_x | 0 \rangle}{(E_0 - E_n)},$$

perturbation sum running over the excited electronic states. Due to the cylindrical symmetry about the linear heavy atom chain, $(L_z L_z/\Delta)$ is zero.

Molecular electric quadrupole moment

$$Q = \frac{e}{2} \left(\sum_{\nu}^{\text{nuclei}} 2 Z_\nu z_\nu^2 - \langle 0 | \sum_{\varepsilon}^{\text{electrons}} (2 z_\varepsilon^2 - x_\varepsilon^2 - y_\varepsilon^2) | 0 \rangle \right)$$

$$= \frac{e h}{8 \pi^2 m_p} \frac{g_\perp}{B} + \frac{4 m c^2}{e} (\chi_\perp - \chi_\parallel) \qquad (5)$$

(In (5) the moment of inertia is expressed by the rotational constant: $I_\perp = h/(8\pi^2 B)$.)

Anisotropy in the second moments of the electron charge distribution

$$\langle 0 | \sum_{\varepsilon}^{\text{electrons}} z_\varepsilon^2 - x_\varepsilon^2 | 0 \rangle = \langle 0 | \sum_{\varepsilon}^{\text{electrons}} z_\varepsilon^2 - y_\varepsilon^2 | 0 \rangle = \sum_{\nu}^{\text{nuclei}} Z_\nu z_\nu^2 - \frac{h}{8\pi^2 m_p} \frac{g_\perp}{B} - \frac{4 m c^2}{e^2} (\chi_\perp - \chi) . \quad (6)$$

(For the evaluation of this expression the knowledge of the equilibrium structure of the nuclear chain is required. Here we use Costains r_s-structure [19] shown in Figure 2. Deviations between the equilibrium distances and r_e-distances may be on the order of 0.005 Å. This leads to the estimated uncertainties of 0.2 Å^2 in the sums $\sum_\nu Z_\nu z_\nu^2$ (first row in Table 7).)

Table 3. HCCC^{14}N Zeeman splittings with respect to the hypothetical rigid rotor frequency. The latter is deduced from the zero field hyperfine pattern. As in DCCC^{14}N, albeit slightly less effective, the magnetic field tends to uncouple the spin of the quadrupole nucleus (here ^{14}N) and the overall rotation. Therefore the limiting J-, M_J-, and M_I-values (here the index I refers to the ^{14}N spin) are used to designate the states. Due to the stronger ^{14}N quadrupole coupling constant, the $M_I = \pm 1$ doublet splittings are larger and in many cases they are well resolved. The satellite frequencies and intensity weighted average frequencies are calculated from the molecular parameters listed in Tables 5 and 8 as described in the text. For ^{14}N, $g_I = 0.4036$ was taken from [27]. Spin-rotation coupling and ^{14}N nuclear shielding was neglected. In the last column we give the differences between the calculated satellite frequencies (or intensity weighted average frequencies) and the observed peak frequencies.

$J \rightarrow J'$ ν_{center} (MHz) ΔM_J, H[Gauß]	$(\nu_H - \nu_{center})$ exp. (kHz)	M_J	M'_J	$M_I(^{14}N)$	rel. int.	$(\nu_H - \nu_{center})$ calc. (kHz)	$(\nu_H - \nu_{center})$ calc. average (kHz)	$\nu_{exp} - \nu_{calc.\,av.}$ (kHz)
$0 \rightarrow 1$	−358.5	0	0	1	33	−362.4	−362.4	3.9
9098.117 MHz	−223.0	0	0	−1	33	−225.9	−225.9	2.9
$\Delta M_J = 0$, 18818 G	961.0	0	0	0	33	958.3	958.3	2.7
$0 \rightarrow 1$	−870.0	0	−1	0	50	−873.9	−873.9	3.9
9098.117 MHz	−341.0	0	−1	1	50	−342.9	−342.9	1.9
$\Delta M_J = \pm 1$, 18815 G	−140.0	0	−1	−1	50	−159.6	−143.0	3.0
		0	1	0	50	−126.3		
	455.0	0	1	1	50	451.5	451.5	3.5
	683.0	0	1	−1	50	681.2	681.2	1.8
$1 \rightarrow 2$	−391.5	1	1	−1	20	−393.1	−392.1	1.6
18196.217 MHz	−324.6	1	1	1	20	−326.1	−326.1	1.5
$\Delta M_J = 0$, 18889 G	−245.5	0	0	0	27	−247.9	−247.9	2.4
	−184.0	−1	−1	−1	20	−186.1	−186.1	2.1
	−148.3	−1	−1	1	20	−144.9	−144.9	−3.4
	84.3	0	0	−1	27	74.6	84.5	−0.2
		0	0	1	27	94.4		
	740.9	1	1	0	20	738.7	738.7	2.2
	989.5	−1	−1	0	20	989.2	989.2	0.3
$1 \rightarrow 2$	−843.7	0	−1	0	20	−845.8	−842.1	−1.6
18196.217 MHz		1	0	−1	10	−831.3		
$\Delta M_J = \pm 1$, 18889 G	−719.0	1	0	1	10	−718.8	−718.8	−0.2
	−519.9	−1	−2	0	33	−519.7	−519.7	−0.2
	−346.5	0	1	0	20	−346.8	−346.8	0.3
	−240.1	−1	−2	−1	33	−244.4	−244.4	4.3
	−179.4	−1	−2	1	33	−180.4	−180.4	1.0
	−131.9	0	−1	1	20	−127.8	−125.1	−5.8
		0	−1	−1	20	−122.4		
	11.3	−1	0	−1	10	10.9	10.9	−0.4
	92.7	−1	0	1	10	77.3	94.8	−2.1
		1	2	0	33	97.7		
	251.9	1	2	−1	33	252.3	252.3	−0.4
	368.5	1	2	1	33	369.0	369.0	−0.5
	498.5	0	1	1	20	487.1	500.0	−1.5
		0	1	−1	20	512.9		
	837.5	1	0	0	10	837.7	837.7	−0.2
	1587.3	−1	0	0	10	1587.2	1587.2	0.1

Table 4. DCCC^{14}N Zeeman splittings with respect to the hypothetical rigid rotor center frequency of the hyperfine pattern at zero field. The magnetic field effectively uncouples the spins of both quadrupole nuclei from the overall rotation (compare also Tables 2 and 3) and the quantum numbers of the uncoupled representation $|J, M_J, I_{(D)}, M_{(D)}, I_{(^{14}N)}, M_{(^{14}N)}\rangle$ are used to designate the state. In DCCC^{14}N spin-rotation coupling was included in the calculation ($C_{(N)} = 1.1(2)$ kHz, $C_{(D)} = -0.1(4)$ kHz taken from [23]. Abbreviations are as in Table 2 and 3).

$J \rightarrow J'$ ν_{center} [MHz] ΔM_J, H[Gauß]	$(\nu_H - \nu_{center})$ exp. [kHz]	M_J	M_J'	M_I (^{14}N)	M_I (D)	rel. int.	$(\nu_H - \nu_{center})$ calc. [kHz]	$(\nu_H - \nu_{center})$ average [kHz]	$\nu_{exp} - \nu_{calc.av.}$ [kHz]
$0 \rightarrow 1$	−396.2	0	0	1	0	33	−399.4	−399.4	3.2
8443.161 MHz	−337.2	0	0	1	−1	33	−341.0	−341.0	3.7
$\Delta M_J = 0$, 18813 G		0	0	1	1	33	−340.9		
	−264.4	0	0	−1	0	33	−262.8	−262.8	−1.6
	−203.0	0	0	−1	−1	33	−204.3	−204.2	1.2
		0	0	−1	1	33	−204.1		
	919.8	0	0	0	0	33	919.7	919.7	0.1
	979.7	0	0	0	−1	33	977.0	977.1	3.6
		0	0	0	1	33	977.1		
$0 \rightarrow 1$	−863.0	0	−1	0	−1	17	−874.5	−864.8	1.8
8443.161 MHz		0	−1	0	1	17	−874.5		
$\Delta M_J = \pm 1$, 18816 G		0	−1	0	0	17	−845.6		
	−335.5	0	−1	1	−1	16	−345.4	−335.6	0.1
		0	−1	1	1	16	−345.4		
		0	−1	1	0	16	−316.2		
	−140.5	0	−1	−1	−1	17	−160.7	−142.8	2.3
		0	−1	−1	1	17	−160.7		
		0	1	0	−1	17	−144.5		
		0	1	0	1	17	−144.0		
		0	−1	−1	0	17	−131.0		
		0	1	0	0	17	−115.6		
	441.9	0	1	1	−1	17	432.6	442.7	−0.8
		0	1	1	1	17	433.0		
		0	1	1	0	17	462.5		
	670.9	0	1	−1	−1	16	659.8	669.4	1.5
		0	1	−1	1	16	660.2		
		0	1	−1	0	16	688.2		
$1 \rightarrow 2$	−422.0	−1	−1	1	0	20	−424.0	−424.0	2.0
16886.309 MHz	−371.7	−1	−1	1	−1	20	−374.4	−368.9	−2.7
$\Delta M_J = 0$, 18888 G		−1	−1	1	1	20	−374.4		
		1	1	1	0	20	−358.0		
	−307.7	1	1	1	−1	20	−307.9	−307.8	0.1
		1	1	1	1	20	−307.8		
	−237.0	0	0	0	−1	26	−252.8	−240.3	3.3
		0	0	0	1	26	−252.8		
		0	0	0	0	26	−237.8		
		−1	−1	−1	0	20	−217.6		
	−174.0	1	1	−1	0	20	−176.9	−170.5	−3.5
		−1	−1	−1	1	20	−167.3		
		−1	−1	−1	−1	20	−167.2		
	−125.6	1	1	−1	1	20	−126.5	−126.5	0.9
		1	1	−1	−1	20	−126.5		
	82.0	0	0	−1	−1	26	68.5	84.0	−2.0
		0	0	−1	1	26	68.5		
		0	0	−1	0	26	84.9		
		0	0	1	−1	26	88.4		
		0	0	1	1	26	88.5		
		0	0	1	0	26	104.8		
	706.2	1	1	0	0	20	705.8	705.8	0.4
	752.6	1	1	0	−1	20	755.1	755.1	−2.5
		1	1	0	1	20	755.2		
	954.6	−1	−1	0	0	20	955.3	955.3	−0.7
	1003.0	−1	−1	0	−1	20	1004.6	1004.6	−1.6
		−1	−1	0	1	20	1004.7		

Table 4 (continued)

$J \rightarrow J'$ ν_{center} [MHz] ΔM_J, H[Gauß]	$(\nu_H - \nu_{center})$ exp. [kHz]	M_J	M'_J	M_I (^{14}N)	M_I (D)	rel. int.	$(\nu_H - \nu_{center})$ calc. [kHz]	$(\nu_H - \nu_{center})$ average [kHz]	$\nu_{exp} - \nu_{calc.\,av.}$ [kHz]
$1 \rightarrow 2$	−846.5	0	−1	0	1	10	−849.8	−849.7	3.2
16886.309 MHz		0	−1	0	−1	10	−849.6		
$\Delta M_J = \pm 1$, 18888 G	−680.0	1	0	1	−1	3	−684.6	−684.5	4.5
		1	0	1	0	3	−684.4		
	−505.5	−1	−2	0	−1	20	−515.1	−510.7	5.2
		−1	−2	0	1	20	−514.9		
		−1	−2	0	0	20	−502.0		
	−371.4	0	1	0	−1	10	−367.4	−367.3	−4.2
		0	1	0	1	10	−367.1		
	−231.0	−1	−2	−1	−1	20	−239.2	−234.8	3.8
		−1	−2	−1	1	20	−238.9		
		−1	−2	−1	0	20	−226.4		
	−166.3	−1	−2	1	−1	20	−177.2	−173.0	6.7
		−1	−2	1	1	20	−176.9		
		−1	−2	1	0	20	−164.8		
	−124.7	0	−1	1	−1	10	−133.4	−129.8	5.1
		0	−1	1	1	10	−133.3		
		0	−1	−1	−1	10	−126.4		
		0	−1	−1	1	10	−126.2		
	25.0	−1	0	1	0	3	24.1	26.4	−1.4
		−1	0	−1	−1	3	27.5		
		−1	0	−1	1	3	27.6		
	87.5	1	2	0	−1	20	84.6	89.6	−2.1
		1	2	0	1	20	84.7		
		−1	0	1	−1	3	95.3		
		−1	0	1	1	3	95.4		
		1	2	0	0	20	97.6		
	240.9	1	2	−1	−1	20	237.5	242.0	−1.1
		1	2	−1	1	20	237.6		
		1	2	−1	0	20	250.9		
	359.1	1	2	1	−1	20	356.4	360.7	−1.6
		1	2	1	1	20	356.5		
		1	2	1	0	20	369.2		
	488.4	0	1	1	−1	10	465.0	489.2	−0.8
		0	1	1	1	10	465.2		
		0	1	−1	−1	10	488.5		
		0	1	−1	1	10	488.7		
		0	1	1	0	10	503.1		
		0	1	−1	0	10	525.8		
	800.5	1	0	0	0	3	798.5	798.5	2.0
	875.1	1	0	0	−1	3	869.4	869.6	5.5
		1	0	0	1	3	869.7		
	1528.7	−1	0	0	0	3	1530.3	1530.3	−1.6
	1599.2	−1	0	0	−1	3	1601.5	1601.6	−2.4
		−1	0	0	1	3	1601.6		

Second moments of the electron charge distribution and diamagnetic and paramagnetic susceptibilities

$$\langle 0 | \sum_{\varepsilon}^{\text{electrons}} x_\varepsilon^2 | 0 \rangle = -\frac{2 m c^2}{e^2} \chi_\parallel , \tag{7}$$

$$\langle 0 | \sum_{\varepsilon}^{\text{electrons}} z_\varepsilon^2 | 0 \rangle = -\frac{2 m c^2}{e^2} (2\chi_\perp - \chi_\parallel) - \frac{h}{8\pi^2 m_p} \frac{g_\perp}{B} + \sum_{\nu}^{\text{nuclei}} Z_\nu z_\nu^2 , \tag{8}$$

$$\chi_\perp^{(d)} = -\frac{e^2}{4 m c^2} \langle 0 | \sum_{\varepsilon}^{\text{electrons}} y_\varepsilon^2 + z_\varepsilon^2 | 0 \rangle = -\frac{e^2}{4 m c^2} \langle 0 | \sum_{\varepsilon}^{\text{electrons}} x_\varepsilon^2 + z_\varepsilon^2 | 0 \rangle \tag{9a}$$

$$= \chi_\perp + \frac{e^2}{4 m c^2} \left(\frac{h}{8\pi^2 m_p} \frac{g_\perp}{B} - \sum_{\nu}^{\text{nuclei}} Z_\nu z_\nu^2 \right) ,$$

$$\chi^{(d)} = -\frac{e^2}{2mc^2}\langle 0 | \sum_{\varepsilon}^{\text{electrons}} x_\varepsilon^2 | 0 \rangle$$

$$= -\frac{e^2}{2mc^2}\langle 0 | \sum_{\varepsilon}^{\text{electrons}} y_\varepsilon^2 | 0 \rangle = \chi_\parallel , \qquad (9\,b)$$

$$\chi_\perp^{(p)} = -\frac{e^2}{2m^2c^2}\left(\frac{L_x L_x}{\Delta}\right) = -\frac{e^2}{2m^2c^2}\left(\frac{L_y L_y}{\Delta}\right) \qquad (10\,a)$$

$$= -\frac{e^2}{4mc^2}\left(\frac{h}{8\pi^2 m_p}\cdot\frac{g_\perp}{B} - \sum_{\nu}^{\text{nuclei}} Z_\nu z_\nu^2\right), \qquad (10\,a)$$

$$\chi^{(p)} = -\frac{e^2}{2m^2c^2}\left(\frac{L_z L_z}{\Delta}\right) = 0 . \qquad (10\,b)$$

For the evaluation of these expressions $\chi_\perp$ and $\chi_\parallel$ must be known individually. Since the rotational Zeeman effect experiment only yields the susceptibility anisotropy, additional information is required. As such independent information one usually takes the bulk susceptibility, $\chi = (\chi_\parallel + 2\chi_\perp)/3$. Unfortunately no experimental value for the bulk susceptibility of Cyanoacetylene is available at present, but in our opinion it is possible to estimate its value from the experimental value for Acetylene,

$$\chi_{(H-C\equiv C-H)} = -12.6\cdot 10^{-6}\,\text{erg G}^{-2}\,\text{mole}^{-1} ,$$

and from the changes that are observed when H− is replaced by −C≡N in other molecules. In Table 6 we have listed some examples. All values are taken from ref. [20]. From Table 6 we note that, if the substitution takes place at an asymmetric frame, an increment of typically $-10.3\cdot 10^{-6}\,\text{erg G}^{-2}\,\text{mole}^{-1}$ is observed. In such cases, however, the increment includes a positive "paramagnetic" contribution associated with electronic angular momentum perturbation sums. Due to the cylindrical symmetry such a paramagnetic contribution is not present in our case. Thus, as expected from the higher symmetry at the "sp^3-hybridized" C-atom, the increment for the change from CH_4 to $CH_3-C\equiv N$ is considerably more negative and we take its value to extrapolate from H−C≡C−H to H−C≡C−C≡N:

$$\chi_{(H-C\equiv C-C\equiv N)} \approx \chi_{(H-C\equiv C-H)} - 16\cdot 10^{-6}\,\text{erg G}^{-2}\,\text{mole}^{-1}$$
$$= -28.6\cdot 10^{-6}\,\text{erg G}^{-2}\,\text{mole}^{-1} .$$

All derived molecular parameters in the lower part of Table 7 have been calculated with this extrapolated bulk value. Since Cyanoacetylene has a rather large electric dipole moment of 3.724(3) D

H — C≡C — C≡N
1.057 1.205 1.378 1.159 Å

Fig. 2. r_s-structure of Cyanoacetylene [19] which was used to further evaluate the Zeeman data presented in Table 5. The r_s-distances typically agree within 0.005 Å with the equilibrium distances. As z-axis of the molecular coordinate system we use the C_∞ axis of the equilibrium configuration.

Table 5. Rotational constants, molecular $g_\perp$-values and molecular susceptibility anisotropies $\chi_\perp - \chi_\parallel$ for the vibronic ground state of the four isotopic species of Cyanoacetylene.

	$HCCC^{15}N$	$HCCC^{14}N$	$DCCC^{15}N$	$DCCC^{14}N$
B/[MHz]	4416.752	4549.056	4100.381	4221.579
$g_\perp$	−0.020269(53)	−0.021302(48)	−0.019469(57)	−0.020683(12)
$(\chi_\perp - \chi_\parallel)/(10^{-6}\,\text{erg G}^{-2}\,\text{mole}^{-1})$	11.815(73)	11.863(61)	12.013(69)	11.970(55)

Table 6. Bulk susceptibilities of those pairs of molecules which were used to derive the bulk susceptibility increment $\Delta\chi_{bulk}$ for the H/CN-replacement. (Values are in units of 10^{-6} erg G^{-2} $mole^{-1}$ and were taken from [20].)

Molecule		χ_{bulk}	Molecule		χ_{bulk}	$\Delta\chi_{bulk}$
Methane	CH_4	−12.27	Acetonitrile	CH_3CN	−28.0	−15.73
Acetaldehyd	C_2H_4O	−22.7	Pyruvinitrile	CH_3COCN	−33.2	−10.5
Ethane	C_2H_6	−27.4	Propionitrile	C_2H_5CN	−38.5	−11.1
Propane	C_3H_8	−40.5	Butyronitrile	C_3H_7CN	−49.5	−9.0
Benzene	C_6H_6	−54.84	Benzonitrile	C_6H_5CN	−65.19	−10.35
Toluene	C_7H_8	−66.11	α-Tolunitrile	C_7H_7CN	−76.87	−10.76
Naphthalene	$C_{10}H_8$	−91.9	α-Naphthonitrile	$C_{10}H_7CN$	−103.3	−11.4
Naphthalene	$C_{10}H_8$	−91.9	β-Naphthonitrile	$C_{10}H_7CN$	−101.0	−9.1

Table 7. Molecular vibronic ground state properties which may be derived (see (5) through (10)) from the experimental values listed in Table 5, the r_s-structure (Fig. 2) and the extrapolated value of $-28.6 \cdot 10^{-6}$ erg G^{-2} mole^{-1} for the bulk susceptibility. An uncertainty of ± 2 units was assumed for this value for error propagation analysis of the final data. Since r_e-distances should be used in (2) through (10) of the text, an uncertainty of 0.2 Å^2 in the sum $\sum_v Z_v z_v^2$ was used for error propagation analysis (compare text). The uncertainty in $\langle 0 | \sum_\varepsilon x_\varepsilon^2 | 0 \rangle$ is entirely due to the assumed uncertainty of two units in χ_{bulk}. In the uncertainty of $\langle 0 | \sum_\varepsilon z_\varepsilon^2 | 0 \rangle$ the assumed uncertainties in $\sum_v Z_v z_v^2$ and in χ_{bulk} enter with approximately equal weight.

	HCCC^{15}N	HCCC^{14}N	DCCC^{15}N	DCCC^{14}N
$\sum_v^{\text{nuclei}} Z_v z_v^2$	59.98(20) Å^2	59.84(20) Å^2	59.79(20) Å^2	59.76(20) Å^2
$Q_\parallel$	2.312(85) $\cdot 10^{-26}$ esu cm^2	2.141(77) $\cdot 10^{-26}$ esu cm^2	2.153(89) $\cdot 10^{-26}$ esu cm^2	1.740(42) $\cdot 10^{-26}$ esu cm^2
$Q_\parallel$ corr.	2.05(9) $\cdot 10^{-26}$ esu cm^2	2.14(8) $\cdot 10^{-26}$ esu cm^2	2.07(9) $\cdot 10^{-26}$ esu cm^2	2.16(4) $\cdot 10^{-26}$ esu cm^2
$\langle 0 \mid \sum_v z_\varepsilon^2 - x_\varepsilon^2 \mid 0 \rangle$	59.49(22) Å^2	59.38(22) Å^2	59.34(22) Å^2	59.42(22) Å^2
$\chi_\perp$	$-24.66(202)$ $\cdot 10^{-6}$ erg G^{-2} mole^{-1}	$-24.65(202)$ $\cdot 10^{-6}$ erg G^{-2} mole^{-1}	$-24.60(202)$ $\cdot 10^{-6}$ erg G^{-2} mole^{-1}	$-24.61(202)$ $\cdot 10^{-6}$ erg G^{-2} mole^{-1}
$\chi_\parallel$	$-36.48(205)$ $\cdot 10^{-6}$ erg G^{-2} mole^{-1}	$-36.51(204)$ $\cdot 10^{-6}$ erg G^{-2} mole^{-1}	$-36.61(205)$ $\cdot 10^{-6}$ erg G^{-2} mole^{-1}	$-36.58(204)$ $\cdot 10^{-6}$ erg G^{-2} mole^{-1}
$\chi_\perp^{(p)}$	264.29(87) $\cdot 10^{-6}$ erg G^{-2} mole^{-1}	263.90(87) $\cdot 10^{-6}$ erg G^{-2} mole^{-1}	263.87(88) $\cdot 10^{-6}$ erg G^{-2} mole^{-1}	264.15(85) $\cdot 10^{-6}$ erg G^{-2} mole^{-1}
$\chi_\parallel^{(p)}$	0.0 $\cdot 10^{-6}$ erg G^{-2} mole^{-1}	0.0 $\cdot 10^{-6}$ erg G^{-2} mole^{-1}	0.0 $\cdot 10^{-6}$ erg G^{-2} mole^{-1}	0.0 $\cdot 10^{-6}$ erg G^{-2} mole^{-1}
$\chi_\perp^{(d)}$	$-288.96(290)$ $\cdot 10^{-6}$ erg G^{-2} mole^{-1}	$-288.54(289)$ $\cdot 10^{-6}$ erg G^{-2} mole^{-1}	$-288.46(290)$ $\cdot 10^{-6}$ erg G^{-2} mole^{-1}	$-288.76(287)$ $\cdot 10^{-6}$ erg G^{-2} mole^{-1}
$\chi_\parallel^{(d)}$	$-36.48(205)$ $\cdot 10^{-6}$ erg G^{-2} mole^{-1}	$-36.51(204)$ $\cdot 10^{-6}$ erg G^{-2} mole^{-1}	$-36.61(205)$ $\cdot 10^{-6}$ erg G^{-2} mole^{-1}	$-36.58(204)$ $\cdot 10^{-6}$ erg G^{-2} mole^{-1}
$\langle 0 \mid \sum z_\varepsilon^2 \mid 0 \rangle$	63.79(31) Å^2	63.69(31) Å^2	63.66(31) Å^2	63.73(31) Å^2
$\langle 0 \mid \sum x_\varepsilon^2 \mid 0 \rangle$	4.30(23) Å^2	4.30(23) Å^2	4.31(23) Å^2	4.31(23) Å^2

[22], the molecular electric quadrupole moment depends on the origin of the reference system. For better comparison we have therefore also listed "corrected" molecular electric quadrupole moments, all referred to the location of the center of mass of the most abundant isotopic species.

Discussion

In the first section of our discussion we will briefly comment on the appearent discrepancy between the Deuterium quadrupole coupling constant determined here and the values derived earlier from the microwave Fourier transform experiments [5, 5a]. We are convinced that the difference is mainly due to the fact that in the Fourier transform experiment the line peaks of the power spectra were directly used to fit the coupling constant. Since in such a treatment the dispersion wings of closely neighboured lines are added before squaring, they tend to compensate in the region between the lines, thus producing the typical asymmetric line shapes shown in Fig. 1 of [5]. In this context it should be noted that the corresponding shifts of the peak frequencies are more pronounced if the lines differ in intensity. A simulation shows that, even though the peaks appear to be perfectly separated, the observed splittings may be on the order of 10 kHz larger than the actual differences of the molecular resonance frequencies. This would account almost quantitatively for the difference in the reported constants. Actually the more detailed evaluation of the Fourier transform spectra is further complicated through the phase shifts introduced by the time delay between the end of the exciting pulse and the start of data sampling.

Since Dreizler and coworkers are developing a considerably improved scheme for the evaluation of Fourier transform spectra of closely spaced multiplets, a very accurate value for the Deuterium-quadrupole coupling constant in Cyanoacetylene may be expected in the near future. It should also be noted in this context that recently Tack and

Table 8. Experimental ^{14}N and D nuclear electric quadrupole coupling constants in Cyanoacetylene. Our values were obtained from a least squares fit of the calculated splittings (numerical diagonalization of the corresponding Hamiltonian matrix) to the observed Hfs-Zeeman splittings. The discrepancy between our values and those derived from the microwave Fourier transform experiments is discussed in the text.

	HCCC^{14}N kHz	DCCC^{14}N kHz	DCCC^{15}N kHz
eQq (^{14}N)	−4318.7(49) [a] −4322.0(46) [e]	−4316.0(30) [c] −4318.0(1) [d] −4313.0(38) [e]	
eQq (D)		228.8(55) [c] 203.5(15) [d] 198.2(46) [e]	229.6(48) [b] 197.3(56) [e]

[a] [21]; [b] [5]; [c] [5a]; [d] [23]; [e] this work.

Kukolich [23] have carried out a molecular beam electric resonance experiment on Cyanoacetylene. Their value for the Deuterium quadrupole coupling constant $eQq = (203.5 \pm 1.5)$ kHz coincides with our value within the experimental uncertainties.

We now turn to the comparison of the molecular parameters determined here with the corresponding ab initio SCF values calculated using (3-21 G) and (6-31 G**) basis sets [6]. We first note the good agreement between the molecular electric quadrupole moments: $Q_{\parallel} = 2.199 \cdot 10^{-26}$ esu cm^2 ((3-21 G) basis set) and $Q_{\parallel} = 2.345 \cdot 10^{-26}$ esu cm^2 ((6-31 G**) basis set) as compared to our experimental value $Q_{\parallel} = (2.14 \pm 0.09) \cdot 10^{-26}$ esu cm^2. A comparison of the second moments of the electron charge distribution, however, indicates that this agreement is possibly the result of a compensation of errors. With $\langle 0 | \sum_{\varepsilon} x_{\varepsilon}^2 | 0 \rangle = \langle 0 | \sum_{\varepsilon} y_{\varepsilon}^2 | 0 \rangle = 4.77$ Å^2 ((3-21 G) basis set) and 4.69 Å^2 ((6-31 G**) basis set) these values are about 0.4 Å^2 larger than our value of 4.3 Å^2. Admittedly our value involves the estimate of the bulk susceptibility. But if we took $\langle 0 | \sum_{\varepsilon} x_{\varepsilon}^2 | 0 \rangle = 4.77$ Å^2 from the ab initio work and reversed the process of calculation, we would arrive at $\chi_{\parallel} = -40.47 \cdot 10^{-6}$ erg G^{-2} mole^{-1} (see (9b)) and this value, if combined with the experimental value for the susceptibility anisotropy $\chi_{\perp} - \chi_{\parallel} = (11.95 \pm 0.08) \cdot 10^{-6}$ erg G^{-2} mole^{-1} (average value over the four isotopic species, see Table 5) would lead to a bulk susceptibility of $-32.52 \cdot 10^{-6}$ erg G^{-2} mole^{-1}. This would correspond to a H−/−C≡N replacement increment of $-19.92 \cdot 10^{-6}$ erg G^{-2} mole^{-1} for the step from H−C≡C−H to H−C≡C−C≡N, rather than the increment of $-16 \cdot 10^{-6}$ erg G^{-2} mole^{-1} deduced from the molecular pair Methane/Acetonitrile.

Even though the CH_3-frame still lacks perfect cylindrical symmetry, we find it hard to believe that a paramagnetic contribution of +4 units should be present in the −C≡N region of Acetonitrile. Such an effect would be of the same order as the ring current quenching effects observed in Fluorine substituted Benzenes and Pyridines [13, 24], and this appears unlikely to us. We therefore suppose that the wavefunctions used to calculate $\langle 0 | \sum x_{\varepsilon}^2 | 0 \rangle$ in the ab initio work possibly overemphasize the contribution of the outer part of the electron cloud by about 0.4 Å^2. An accurate experimental determination of the bulk susceptibility of Cyanoacetylene would therefore be of great interest to settle this problem.

Finally we would like to comment briefly on the currently accepted value for the "nuclear quadrupole moment" of ^{14}N, $Q(^{14}N) = 1.59 \cdot 10^{-26}$ cm^2 [25]. From the microwave data for the quadrupole coupling constants in H−C≡N, $eQq = (-4709 \pm 1.3)$ kHz [26] and H−C≡C−C≡N, $eQq = (4318.0 \pm 0.1)$ kHz [23], on the one hand, and from the ab initio SCF field gradients at the ^{14}N nucleus reported in ref. [6], on the other hand, (q(H−C≡N) = 0.9742 atomic units and q(H−C≡C−C≡N) = 0.9064 atomic units) one obtaines quite consistently $Q(^{14}N) = 1.99 \cdot 10^{-26}$ cm^2, which is very close to the old value of $2 \cdot 10^{-26}$ cm^2 given in [27]. Of course, in view of our slight restraints with respect to the ab initio values for the second moments of the electron charge distribution, also the ^{14}N nuclear quadrupole moment may still be open for discussion. We may note, however, that Ha himself, on the basis of further ab initio calculations on NH_3 now favours a value of $1.95 \cdot 10^{-26}$ cm^2 for $Q(^{14}N)$ [28].

Acknowledgement

We gratefully acknowledge the financial support by Deutsche Forschungsgemeinschaft and Fonds der chemischen Industrie, and we would like to thank Prof. H. Dreizler for carefully reading the manuscript. All numerical calculations have been carried out at the computer center of the University of Kiel.

[1] A. A. Westenberg and E. Bright Wilson Jr., J. Amer. Chem. Soc. **72,** 199 (1950).
[2] B. E. Turner, Astrophys. J. **163,** L35 (1971).
[3] M. Morris, B. W. Turner, P. Palmer, and B. Zuckerman, Astrophys. J. **205,** 82 (1976).
[4] E. Churchwell, G. Winnewisser, and C. M. Walmsley, Astron. Astrophys. **67,** 139 (1978).
[5] E. Fliege, G. Bestmann, M. Andolfatto, and H. Dreizler, Z. Naturforsch. **36 a,** 1126 (1981).
[5a] E. Fliege, H. Dreizler, and B. Kleibömer, J. Mol. Struct. **97,** 225 (1983).
[6] Tae-Kyu Ha and Minh Tho Nguyen, Z. Naturforsch. **37 a,** 1272 (1982).
[7] W. H. Flygare and R. C. Benson, Mol. Phys. **20,** 225 (1971).
[8] W. H. Flygare, Chem. Revs. **74,** 653 (1974).
[9] D. H. Sutter and W. H. Flygare, Topics in Currenct Chemistry **63,** 69 (1976).
[10] W. H. Stolze, Dipl.-Thesis, Kiel 1982. Only the $J = 1 \rightarrow J' = 2$ rotational transitions had been measured in 1982. The present work includes the $J = 0 \rightarrow J' = 1$ data obtained after extension of the superheterodyne bridge spectrometer to the X-band region.
[11a] See Ref. [9], Eqs. (I.2), (I.4), and (II.1) through (II.4).
[11b] See Ref. [7], Eqs. (2) through (5) and (24) through (29).
[12] H. Bomsdorf and H. Dreizler, Z. Naturforsch. **38 a,** 1003 (1983).
[13] W. H. Stolze, M. Stolze, D. Hübner, and D. H. Sutter, Z. Naturforsch. **37 a,** 1165 (1982).
[14] M. Stolze, D. Hübner, and D. H. Sutter, J. Mol. Struct. **97,** 243 (1982).
[15] D. H. Sutter, Z. Naturforsch. **26 a,** 1644 (1971).
[16] [9], Chapt. III.
[17] [9], Fig. III.6 and III.13 and corresponding discussion.
[18] K. F. Dössel and D. H. Sutter, Z. Naturforsch. **34 a,** 469 (1979).
[19] C. C. Costain, J. Chem. Phys. **29,** 864 (1958).
[20] Handbook of Chemistry and Physics, 62 Ed., R. C. Weast Ed., CRC Press Inc. Boa Raton, Florida 1982, E-129-132.
[21] R. A. Creswell and G. Winnewisser, J. Mol. Spectr. **65,** 420 (1977).
[22] W. J. Lafferty and F. J. Lovas, J. Phys. Chem. Ref. Data **7,** 441 (1978).
[23] L. M. Tack and S. G. Kukolich, J. Chem. Phys. **78,** 6512 (1983).
[24] D. Hübner, M. Stolze, and D. H. Sutter, Z. Naturforsch. **36 a,** 332 (1981).
[25] See Nuclear Physics A360 (1981). The value was deduced from a comparison of ab initio field gradients and experimental hyperfine structures: C. T. O'Konski and T.-K. Ha, J. Chem. Phys. **49,** 5254 (1968).
[26] F. de Lucia and W. Gordy, Phys. Rev. **187,** 58 (1969).
[27] C. H. Townes and A. L. Schawlow, Microwave Spectroscopy, Dover Publications Inc., New York 1975, p. 644.
[28] Tae-Kyu Ha, private communication of results submitted for publication to Chem. Phys. Letters.